Energy Levels, Lifetimes, and Transition Probabilities for Rb(XXIII)

Min Xu[a], Feng Hu[b,*], Yan Sun[b], Yuewu Pan[b] and Hao Liu[c]

[a]*Key Laboratory of State Ethnic Affairs Commission for Electronic and Information Engineering, Southwest Minzu University, Chengdu 610041, People's Republic of China*
[b]*School of Physics and New Energy, Xuzhou University of Technology, Xuzhou 221018, People's Republic of China*
[c]*Research Center of Laser Fusion, China Academy of Engineering Physics, Mianyang 621900, People's Republic of China*

Energy levels, radiative rates, lifetimes, hyperfine structures and Landé g_J-factors for electric–dipole (E1), electric–quadrupole (E2), magnetic–dipole (M1), and magnetic–quadrupole (M2) transitions among the lowest 41 levels belonging to the $n = 3$ states ($1s^2 2s^2 2p^6$)$3s^2 3p^3$, $3s 3p^4$, and $3s^2 3p^2 3d$ in Rb(XXIII) are calculated through the multiconfiguration Dirac–Hartree–Fock method. High-accuracy calculations have been performed as benchmarks in the request for accurate treatments of relativity, electron correlation, and quantum electrodynamic effects in multi-valence-electron systems. The calculated energy levels are in excellent agreement with the experimental results and the theoretical ones, wherever available. The calculated values including core–valence correction are found to be in good agreement with other theoretical and experimental values. The present results are reported as benchmarks for future calculations and measurements.

topics: energy levels, radiative rates, transition probabilities

1. Introduction

The most frequent use of Rb is in the field of astrophysics and atomic physics. The formation of the rubidium resonance lines has been used to investigate the temperature and abundance of elements in cool stars [1]. Rubidium is a key element for the slow neutron-capture mechanisms-process diagnostic [2]. The absorption spectroscopy of rubidium was performed to improve the accuracy of the atomic clock [3]. Rubidium vapor was pumped to study proton polarization produced in the process of polarized electron capture [4]. Experimental spectra are mainly from low ionized Rb ions, and there were no experimental results for Rb(XXI)–Rb(XXXVII) (except four ions) [5]. The energy levels and transition probabilities of Rb(XXI)–Rb(XXXVII) quoted by the Atomic Spectra Database of the National Institute of Standards and Technology (NIST ASD) were obtained from the predictions of isoelectronic sequences [6]. For Rb(XXIII), no measurements of the spectrum have been made, and the study was mainly from phosphorus isoelectronic sequence. By investigating magnetic dipole transition within the $3s^2 3p^3$ ground state, the ground state levels, wavelengths, and transition probabilities were predicted

by Sugar and Kaufman [7]. Later, four levels in the $3s^2 3p^2 3d$ configuration and wavelengths for transitions to those levels from the ground term were made by Sugar et al. [8]. The multiconfiguration Dirac–Fock technique was used to calculate the transition rates for Rb(XXIII) by Huang [9].

Träbert conducted a critical assessment of theoretical calculations of structure and transition probabilities from an experimenter's perspective [10]. He pointed out that new computations can match the measurement, fill gaps and suggest revisions closely with almost spectroscopic accuracy. These citations of theoretical work as well as the ones for experimental data are certainly incomplete. The citations concerned several P-like ions calculations, and the trend attracted attention. Consequently, limited energy levels or transitions were considered, or selected configurations were discussed [7, 8] and some results were given in a graphic form [9]. There still exist some problems, such as the identification of terms and strong mixing of configurations, which will be discussed in detail in the next part of this paper.

In this paper, the MCDHF method is performed to calculate E1, E2, M1, and M2 wavelengths, oscillator strengths, transition probabilities, and fine-structure levels for Rb(XXIII) using the new release

of the GRASP2K code [11, 12] and the fully relativistic flexible atomic code (FAC) program [13], which was used to check the energy levels. Configurations $(1s^2 2s^2 2p^6)3s^2 3p^3$, $3s3p^4$, and $3s^2 3p^2 3d$ are reported in this calculation. Based on our previous work [14, 15], in this paper, the valence–valence (VV) and core–valence (CV) correlation effects are considered systematically. The Breit interactions (BI) and quantum electrodynamics (QED) effects have been added. This computational approach enables us to present a consistent and improved data set of all-important E1, E2, M1, and M2 transitions of the Rb(XXIII) spectra, which are useful for identifying transition lines in further investigations.

2. Theoretical methods

2.1. MCDHF method

The multiconfiguration Dirac–Hartree–Fock (MCDHF) method has recently been described in great detail by Grant [16]. Hence, we only repeat its essential features here. We start from the Dirac–Coulomb Hamiltonian

$$H_{\text{DC}} = \sum_{i=1}^{N} \left(c\boldsymbol{\alpha}_i \cdot \boldsymbol{p}_i + (\beta_i - 1)c^2 + V_i^N \right) + \sum_{i>j}^{N} \frac{1}{r_{ij}}. \tag{1}$$

Here, V^N is the monopole part of the electron–nucleus Coulomb interaction, α and β are the 4×4 Dirac matrices, and c is the speed of light in atomic units. The atomic state functions (ASFs) describing different fine-structure states are obtained as linear combinations of symmetry-adapted configuration state functions (CSFs):

$$|\gamma J M_J\rangle = \sum_{j=1}^{N_{CSFs}} c_j |\gamma_j J M_J\rangle, \tag{2}$$

where J and M are the angular quantum numbers and P is the parity. Parameter γ_i denotes another appropriate labeling of the configuration state function i, for example, orbital occupancy, and coupling scheme. Normally, the label γ is the same as the label of the dominating CSF. The CSFs are built from products of one-electron Dirac orbitals. In the relativistic self-consistent field (RSCF) procedure, both the radial parts of the Dirac orbitals and the expansion coefficients are optimized to self-consistency. The Breit interaction

$$H_{\text{Breit}} = -\sum_{i<j}^{N} \left[\boldsymbol{\alpha_i} \cdot \boldsymbol{\alpha}_j \frac{\cos\left(\omega_{ij} r_{ij}/c\right)}{r_{ij}} \right.$$
$$\left. + (\boldsymbol{\alpha}_i \cdot \nabla_i)(\boldsymbol{\alpha}_j \cdot \nabla_j) \frac{\cos\left(\omega_{ij} r_{ij}/c\right) - 1}{\omega_{ij}^2 r_{ij}/c^2} \right] \tag{3}$$

was included in the Hamiltonian. The photofrequencies ω_{ij}, used for calculating the matrix elements of the transverse photo-interaction, were taken as the difference of the diagonal Lagrange multipliers associated with the Dirac orbitals.

In the relativistic configuration interaction (RCI) calculation, leading QED corrections [17], self-interaction, and vacuum polarization were also included.

2.2. MBPT method

In the MBPT method implemented in the FAC package [13], the Dirac–Coulomb–Breit Hamiltonian can be written as

$$H_{\text{DCB}} = \sum_{i}^{N} \left(h_d(i) - \frac{Z}{r_i} \right) + \sum_{i<j}^{N} \left(\frac{1}{r_{ij}} + B_{ij} \right), \tag{4}$$

where h_d is the free-electron Dirac Hamiltonian, r_i is the radial coordinate of the electron i, r_{ij} is the distance between the electrons i and j, and Z is the nuclear charge number. The frequency-independent Breit interaction is denoted as B_{ij}.

The H_{DCB} is split up into a model Hamiltonian H_0 and a perturbation V, namely

$$H_0 = \sum_i h_d(i) + U(r_i), \tag{5}$$

$$V = -\sum_i \left(\frac{Z}{r_i} + U(r_i) \right) + \sum_{i<j}^{N} \left(\frac{1}{r_{ij}} + B_{ij} \right). \tag{6}$$

Here, U(r) is approximated by a local central potential and derived from an RSCF calculation. The eigenfunctions of H_0 are divided into a model space M and an orthogonal space N. A non-Hermitian effective Hamiltonian whose eigenvalues are the true eigenenergies of the full Hamiltonian can be constructed in the M space. By solving the generalized eigenvalue problem for the first-order effective Hamiltonian, we can obtain the eigenvalues in the second order. With this method, the CI effects within the M space are included for all orders, while the interaction between M and N is taken into account for the second order. Finally, several small corrections to the Hamiltonian, such as QED, are also included.

2.3. Calculation procedure

The $3s^2 3p^3$, $3s3p^4$, and $3s^2 3p^2 3d$ configurations define the multireference (MR) for the even and odd parities, respectively. As a starting point, MCDHF calculations in the EOL scheme were performed for even and odd states using configuration expansions including all lower states of the same J symmetry and parity, and a Dirac–Coulomb version was used, for the optimization of the orbitals, including BI in a final configuration interaction calculation [16].

The calculations for the even states were based on CSF expansions obtained by allowing single (S) and double (D) substitutions of orbitals in the even MR configurations to an increasingly active set of orbitals. Similarly, the calculations for the odd states were based on CSF expansions obtained by allowing S and D substitutions of orbitals in the odd MR configurations to an increasingly active set of orbitals. A similar calculation procedure has been introduced

in a previous paper [14], thus in the current paper we only give an outline. For P-like ions, the ground and first excited configurations are $3s^23p^3$, and $3s^23p^23d$, respectively. In the first step, the active set (AS) is

$$AS1 = \{3s, 3p, 3d\}. \tag{7}$$

Then, we increase the active set in the following way:

$$AS2 = AS1 + \{4s, 4p, 4d, 4f\}, \tag{8}$$

$$AS3 = AS2 + \{5s, 5p, 5d, 5f, 5g\}, \tag{9}$$

$$AS4 = AS3 + \{6s, 6p, 6d, 6f, 6g\}, \tag{10}$$

$$AS5 = AS4 + \{7s, 7p, 7d, 7f, 7g\}. \tag{11}$$

In our VV method, we set $1s^22s^22p^6$ as our core electrons in the calculation. Then, we considered increasing the principal quantum number n and optimized the orbitals AS1, AS2, AS3, AS4, and AS5.

In the CV model, we set $1s^22s^22p^5$ as our core electrons, then we optimized the layer by n. We generated the CSFs of the form of $1s^22s^22p^5$ ASn, $n = 1$–4. Also, the CSFs of CV have the form of $1s^22s^12p^6$ ASn, $n = 1$–4.

In our MBPT calculation, the $3l^5$, $43l^44l$, and $3l^45l$ configurations are contained in the model space M, and all possible configurations that are generated by SD excitations from the M space are contained in space N.

All calculations were done in jj-coupling. To give a good consistency with the labeling system, we used the NIST ASD and other sources. The GRASP2K procedure JJ2LSJ [18] was used for the transformation of ASFs from a jj-coupled CSF basis into an LSJ-coupled CSF basis for the results.

3. Results and discussion

Results for $(1s^22s^22p^6)3s^23p^3$, $3s3p^4$, and $3s^23p^23d$ configurations of Rb(XXIII) give rise to the low-lying 41 levels listed in Table I, where we compared our results with the experimental data compiled by NIST [6]. The NIST database listed the energies for the 12 out of the present 41 excited-levels in Rb(XXIII). The average values of the difference for MCDHFCV energies of the 41 levels are

- $\left(\frac{|\mathrm{MR} - (n=4)|}{\max(\mathrm{MR}, n=4)} \right)$,
- $0.164\% \left(\frac{|(n=5) - (n=4)|}{\max(n=5, n=4)} \right)$,
- $0.019\% \left(\frac{|(n=6) - (n=5)|}{\max(n=6, n=5)} \right)$,
- $0.005\% \left(\frac{|(n=7) - (n=6)|}{\max(n=7, n=6)} \right)$.

The principal number was limited to $n = 7$. For the VV calculation, it is not very difficult to get convergence for a higher principal number ($n \geq 8$), but for the CV calculation, the convergence is difficult. The number of CSFs would increase very rapidly when we include the $n \geq 8$ orbitals, and it is hard to get convergence. Also, because of the computer calculation limit and the problem of the program
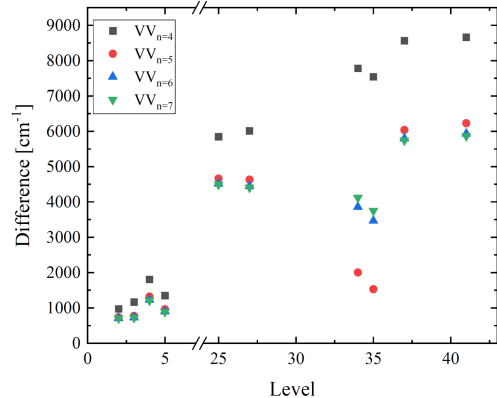
Fig. 1. Energy difference between the valence–valence correlation results and the energies for the 12 out of the lowest 41 levels from NIST.
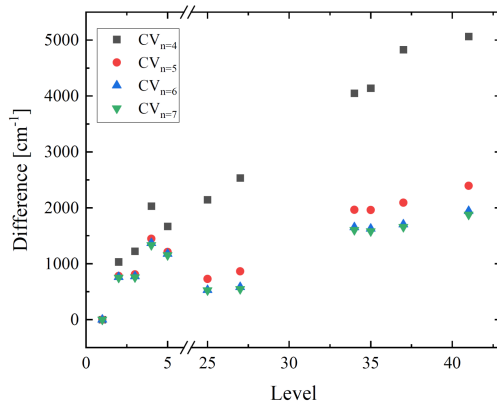
Fig. 2. Description as in Fig. 1, but for the core–valence correlation results.

GRASP2K code itself, we only compare the VV and CV models on an equal footing, as mentioned above.

Figure 1 shows the mean values (with the standard deviation) of the relative differences between VV_n and NIST are 881 and 4728 cm^{-1}. The smallest difference is 750 cm^{-1} lower than NIST ($3s^23p^3\ ^2D_{3/2}$), and the biggest difference can be up to 8660 cm^{-1} ($3s^23p^23d\ (^3P)\ ^2F_{5/2}$). Figure 2 shows the mean values (with the standard deviation) of the relative differences between CV_n and NIST are 997 and 1297 cm^{-1}. This can be treated as a good example of calculations with the necessary correlations included. As can be seen from Figs. 1 and 2, some results considering more configurations are not better than those with fewer configurations. This can be due to configuration mixing. The present results in Fig. 3 are the VV and CV calculations with $n = 7$. For $3s^23p^3$, the VV results agree well with NIST in the range of 0.36% to 0.81%, while the CV results — in the range of 0.47% to 0.87%. For $3s^23p^23d$, the VV results agree well with NIST in the range of 0.36% to 0.53%, while the CV results — in the range of 0.06% to 0.16%. Theoretical results from FAC differ from NIST in the range of -0.62% to 7.46% for $3s^23p^3$ and -0.01% to 1.07% for $3s^23p^23d$.

Energies (in [cm^{-1}]) relative to the ground state for the lowest 41 levels in Rb(XXIII).

TABLE I

Key	Configuration	$VV_{n=4}$	$VV_{n=5}$	$VV_{n=6}$	$VV_{n=7}$	$CV_{n=4}$	$CV_{n=5}$	$CV_{n=6}$	$CV_{n=7}$	Exp.
1	$3s^23p^3\ ^4S_{3/2}$	0	0	0	0	0	0	0	0	0
2	$3s^23p^3\ ^2D_{3/2}$	87452	87213	87188	87182	87509	87258	87240	87228	86478
3	$3s^23p^3\ ^2D_{5/2}$	119584	119191	119150	119140	119642	119228	119193	119174	118418
4	$3s^23p^3\ ^2P_{1/2}$	168148	167661	167572	167551	168370	167788	167711	167674	166341
5	$3s^23p^3\ ^2P_{3/2}$	242608	242222	242161	242147	242928	242469	242435	242411	241259
6	$3s3p^4\ ^4P_{5/2}$	543604	543775	543719	543708	544381	544055	544137	544126	
7	$3s3p^4\ ^4P_{3/2}$	601129	601308	601253	601240	601901	601587	601675	601668	
8	$3s3p^4\ ^4P_{1/2}$	614438	614550	614471	614453	615261	614831	614896	614877	
9	$3s3p^4\ ^2D_{3/2}$	677795	677714	677590	677558	678077	677510	677524	677507	
10	$3s3p^4\ ^2D_{5/2}$	707891	707783	707654	707620	708383	707733	707749	707724	
11	$3s^23p^23d(^3P)^4F_{3/2}$	749880	749327	749186	749153	749316	748321	748237	748242	
12	$3s^23p^23d(^3P)^2P_{3/2}$	768766	768609	768496	768469	768151	767628	767615	767628	
13	$3s3p^4\ ^2S_{1/2}$	772759	772463	772275	772230	772218	771394	771301	771265	
14	$3s^23p^23d(^3P)^4F_{5/2}$	778528	777999	777883	777857	777809	776901	776855	776885	
15	$3s^23p^23d(^1D)^2F_{5/2}$	813237	812654	812534	812506	812619	811707	811649	811675	
16	$3s^23p^23d(^3P)^4F_{7/2}$	825405	825000	824909	824889	824867	824115	824107	824149	
17	$3s^23p^23d(^3P)^4D_{1/2}$	830540	830140	830001	829970	829994	829085	829050	829063	
18	$3s^23p^23d(^3P)^4D_{7/2}$	838508	837946	837828	837801	837960	837039	837004	837036	
19	$3s^23p^23d(^3P)^4D_{3/2}$	847122	846731	846623	846600	846226	845405	845393	845425	
20	$3s^23p^23d(^3P)^4F_{9/2}$	858957	858343	858231	858205	858497	857532	857496	857532	
21	$3s^23p^23d(^3P)^4D_{5/2}$	871619	871102	870996	870973	870786	869912	869885	869921	
22	$3s^23p^23d(^3P)^2P_{1/2}$	878877	878562	878389	878348	878572	877769	877693	877674	
23	$3s^23p^23d(^1D)^2G_{7/2}$	922925	921859	921699	921659	922367	920880	920773	920787	
24	$3s3p^4\ ^2P_{3/2}$	936958	935733	935495	935443	932973	931396	931159	931105	
25	$3s^23p^23d(^3P)^4P_{5/2}$	946079	944891	944748	944721	942372	940958	940760	940754	940230
26	$3s^23p^23d(^1D)^2F_{7/2}$	953887	952937	952786	952748	953444	952117	952031	952049	
27	$3s^23p^23d(^3P)^4P_{3/2}$	960392	959010	958828	958786	956915	955243	954961	954926	954380
28	$3s^23p^23d(^3P)^4P_{1/2}$	966938	965522	965340	965299	963313	961610	961335	961305	
29	$3s^23p^23d(^1D)^2G_{9/2}$	977808	976467	976281	976232	977488	975721	975582	975587	
30	$3s^23p^23d(^1S)^2D_{3/2}$	986026	984227	983922	983850	984567	982400	982013	981958	
31	$3s^23p^23d(^3P)^2D_{5/2}$	1019986	1017896	1017630	1017569	1016460	1014099	1013682	1013618	
32	$3s3p^4\ ^2P_{1/2}$	1020606	1019476	1019274	1019229	1016727	1015244	1015042	1015003	
33	$3s^23p^23d(^1D)^2P_{1/2}$	1050214	1047897	1047584	1047503	1047188	1044513	1044008	1043917	
34	$3s^23p^23d(^1D)^2D_{3/2}$	1051482	1049750	1049523	1049471	1047748	1045665	1045352	1045303	1043700
35	$3s^23p^23d(^1D)^2D_{5/2}$	1055744	1053870	1053628	1053574	1052339	1050160	1049826	1049780	1048200
36	$3s^23p^23d(^1S)^2D_{5/2}$	1076234	1074206	1073878	1073794	1075349	1072876	1072506	1072453	
37	$3s^23p^23d(^3P)^2F_{7/2}$	1092645	1090117	1089876	1089821	1088907	1086172	1085782	1085737	1084080
38	$3s^23p^23d(^1D)^2P_{3/2}$	1110640	1108421	1108121	1108048	1107458	1104918	1104436	1104351	
39	$3s^23p^23d(^1D)^2S_{1/2}$	1124309	1122297	1122001	1121930	1120720	1118361	1117994	1117924	
40	$3s^23p^23d(^3P)^2D_{3/2}$	1155429	1153084	1152764	1152686	1152336	1149651	1149177	1149102	
41	$3s^23p^23d(^3P)^2F_{5/2}$	1163080	1160648	1160353	1160286	1159484	1156814	1156362	1156297	1154420

To see the BI and QED effects more clearly, the contributions to the MCDHF excited energies of the 40 fine-structure levels of Rb(XXIII) in cm^{-1} and percentage are shown in Fig. 4a and b, respectively. The inspection of Fig. 4 reveals that the BI and QED corrections are significant, generally lowering the excited levels by the mean value of 0.61%. As can be seen, the contribution of the Breit interaction is about -1.47%–0.29% (-1956 cm^{-1}–290 cm^{-1}), and the contribution of QED is -0.49%–0.127% (-2692 cm^{-1}–281 cm^{-1}).

The Dirac–Fock wave functions with a minimum number of radial functions are not sufficient to represent the occupied orbitals. Extra
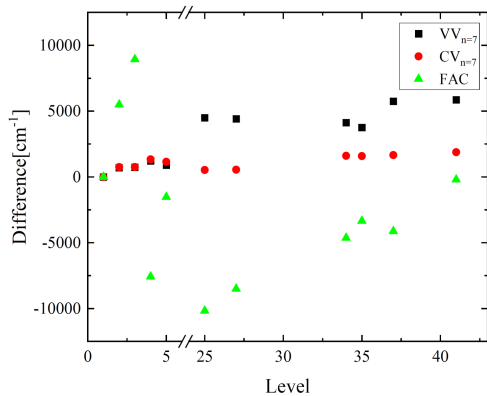
Fig. 3. Differences (in [cm^{-1}]) of various theoretical energies from the NIST-compiled values in Rb(XXIII).
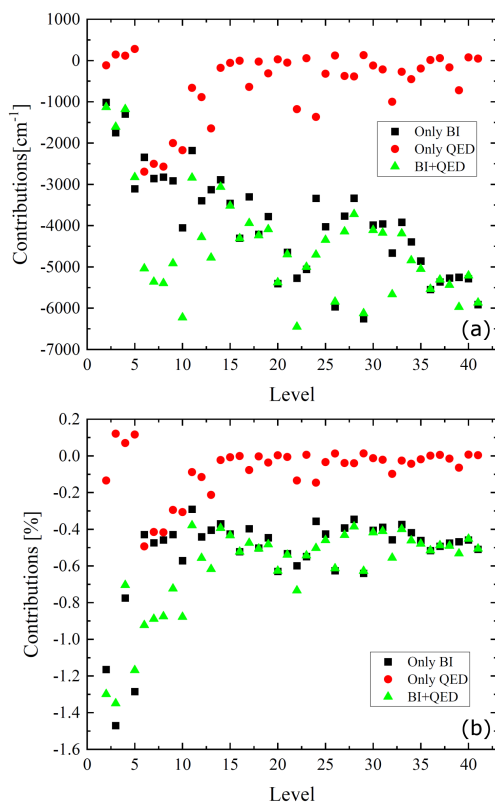
Fig. 4. The effects of the BI and QED corrections on the excitation energies of the Rb(XXIII) configurations obtained from the present MCDHF calculations in [cm^{-1}] (a) and percentage (b).

configurations have to be added to adequately represent electron correlations (i.e., mixing coefficients). These extra configurations are represented by CSFs and must have the same angular momentum and parity as the occupied orbitals [18]. For instance, the $3s^2 3p^3$ $^4S_{3/2}$ level is represented by 0.98 $3s^2 3p^3$ $^4S_{3/2}$ and 0.09 $3s^2 3p^3$ $^2P_{3/2}$. The former two mixing coefficients for the wave functions of the calculated levels are shown in Table II.
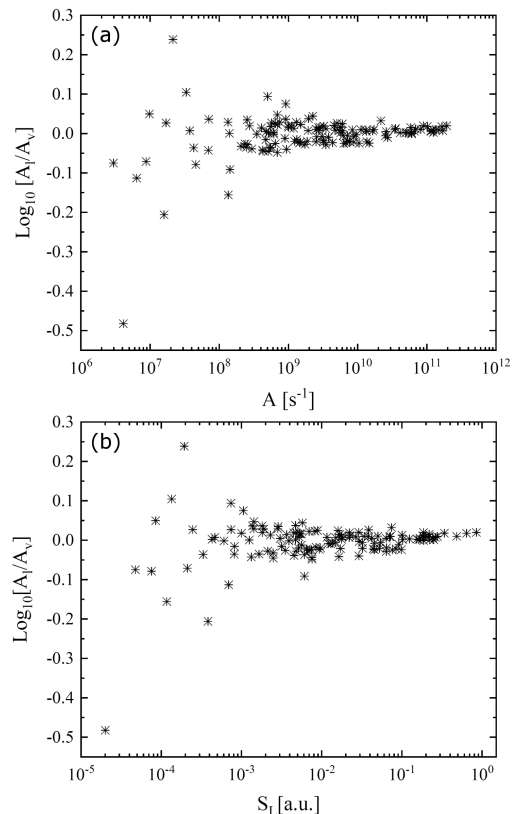
Fig. 5. A scatterplot of $\log(A_l/A_v)$ as a function of transition probability A_l (a) and line strength S_l (b) for the E1 transitions.

The most important contributions to the total wave function of a given level are those from the same configuration. For example, the configuration-mixed wave function for the $3s^2 3p^3 (^4_3 S)^4 S_{3/2}$ level is represented as $3s^2 3p^3$ $^4S_{3/2} = 0.64 3s^2 3p^3$ $^4S_{3/2} + 0.24 3s^2 3p^3$ $^2P_{3/2}$, where 0.64 and 0.24 are contributions. The present and previous results are very close to one another in the description of the configuration-interaction wave functions. Because of the strong mixing, levels 12 and 15, 18 and 23, 28 and 38, 32 and 41 have the same quantum labels in the original output. With the help of JJ2LSJ [18], the levels mentioned above had been adjusted. In the present calculations, the nuclear parameters I, μ_I, and Q are all set to 1. The A_J and B_J values for a specific isotope can be scaled with the tabulated values given in Table II.

Among the calculated wavelengths of transition between the lowest 41 levels in Rb(XXIII), the experimental results data compiled by NIST listed the observed wavelengths for seven E1 transitions. The observed results are from Sugar et al. [8], and the transition rates are from Huang [9]. The accuracy of the calculated CV and VV wavelengths relative to NIST can be assessed using Table III, where the agreement is within 0.10Å for CV. The difference between VV and NIST is in the range of 0.48–0.59 Å, while CV is in the

TABLE II

The LS-composition, A_j, B_j hyperfine interaction constants, and Landé g_J-factors for the lowest 41 levels in Rb(XXIII), $a(b) = a \times 10^b$.

Key	Configuration	Mix	LS-composition	A [MHz]	B [MHz]	g_J
1	$3s^2 3p^3\ {}^4S_{3/2}$	$0.98(1) + 0.09(5)$	$0.64(1) + 0.24(5)$	$1.128(4)$	$1.331(4)$	1.709
2	$3s^2 3p^3\ {}^2D_{3/2}$	$0.78(2) + 0.51(1)$	$0.61(2) + 0.26(1)$	$8.848(3)$	$2.302(4)$	1.174
3	$3s^2 3p^3\ {}^2D_{5/2}$	$0.99(3)$	$0.98(3)$	$3.380(4)$	$-9.019(1)$	1.197
4	$3s^2 3p^3\ {}^2P_{1/2}$	$0.98(4)$	$0.97(4)$	$9.583(4)$	$0.000(0)$	0.663
5	$3s^2 3p^3\ {}^2P_{3/2}$	$0.79(5) + 0.51(2)$	$0.63(5) + 0.26(2)$	$1.921(4)$	$-3.645(4)$	1.243
6	$3s 3p^4\ {}^4P_{5/2}$	$0.90(6) + 0.29(25)$	$0.81(6) + 0.08(25)$	$7.079(4)$	$2.150(4)$	1.560
7	$3s 3p^4\ {}^4P_{3/2}$	$-0.85(7) - 0.31(27)$	$0.74(7) + 0.10(27)$	$3.699(4)$	$-2.362(4)$	1.614
8	$3s 3p^4\ {}^4P_{1/2}$	$0.86(8) + 0.37(13)$	$0.74(8) + 0.13(13)$	$1.781(5)$	$0.000(0)$	2.560
9	$3s 3p^4\ {}^2D_{3/2}$	$0.68(9) - 0.36(7)$	$0.47(9) + 0.13(7)$	$6.231(3)$	$-2.925(4)$	0.992
10	$3s 3p^4\ {}^2D_{5/2}$	$-0.82(10) + 0.42(35)$	$0.67(10) + 0.18(35)$	$7.695(4)$	$-5.209(4)$	1.230
11	$3s^2 3p^2 3d(^3P)^4F_{3/2}$	$0.66(11) - 0.41(9)$	$0.43(11) + 0.17(9)$	$6.008(3)$	$2.341(3)$	0.751
12	$3s^2 3p^2 3d(^3P)^2P_{3/2}$	$0.55(12) - 0.54(11)$	$0.31(12) + 0.30(11)$	$1.015(4)$	$-1.342(3)$	1.011
13	$3s 3p^4 {}^2S_{1/2}$	$0.50(13) + 0.52(32)$	$0.25(13) + 0.26(32)$	$6.577(4)$	$0.000(0)$	1.150
14	$3s^2 3p^2 3d(^3P)^4F_{5/2}$	$0.75(14) + 0.49(21)$	$0.57(14) + 0.24(21)$	$5.463(3)$	$1.410(4)$	1.129
15	$3s^2 3p^2 3d(^1D)^2F_{5/2}$	$-0.63(15) - 0.52(41)$	$0.39(15) + 0.27(41)$	$2.627(4)$	$-1.101(4)$	0.941
16	$3s^2 3p^2 3d(^3P)^4F_{7/2}$	$0.91(16) + 0.29(18)$	$0.83(16) + 0.08(18)$	$9.589(3)$	$8.659(3)$	1.232
17	$3s^2 3p^2 3d(^3P)^4D_{1/2}$	$-0.83(17) - 0.40(13)$	$0.69(17) + 0.17(13)$	$8.182(4)$	$0.000(0)$	0.548
18	$3s^2 3p^2 3d(^3P)^4D_{7/2}$	$-0.64(18) + 0.57(37)$	$0.41(18) + 0.33(37)$	$1.239(4)$	$2.220(4)$	1.243
19	$3s^2 3p^2 3d(^3P)^4D_{3/2}$	$0.85(19) - 0.33(11)$	$0.72(19) + 0.11(11)$	$1.169(4)$	$-1.430(4)$	1.120
20	$3s^2 3p^2 3d(^3P)^4F_{9/2}$	$0.87(20) - 0.47(22)$	$0.76(20) + 0.22(29)$	$1.608(4)$	$-4.559(3)$	1.281
21	$3s^2 3p^2 3d(^3P)^4D_{5/2}$	$0.70(21) - 0.37(14)$	$0.50(21) + 0.14(14)$	$1.662(4)$	$-1.333(4)$	1.205
22	$3s^2 3p^2 3d(^3P)^2P_{1/2}$	$-0.52(22) - 0.52(13)$	$0.28(22) + 0.26(13)$	$1.244(5)$	$0.000(0)$	1.067
23	$3s^2 3p^2 3d(^1D)^2G_{7/2}$	$-0.68(23) + 0.52(18)$	$0.46(23) + 0.27(18)$	$1.739(4)$	$2.743(4)$	1.114
24	$3s 3p^4\ {}^2P_{3/2}$	$0.65(24) + 0.45(12)$	$0.42(24) + 0.19(12)$	$-6.854(3)$	$1.176(4)$	1.193
25	$3s^2 3p^2 3d(^3P)^4P_{5/2}$	$0.81(25) - 0.31(21)$	$0.66(25) + 0.09(21)$	$9.799(3)$	$2.060(3)$	1.504
26	$3s^2 3p^2 3d(^1D)^2F_{7/2}$	$0.58(26) + 0.59(23)$	$0.33(26) + 0.35(23)$	$1.325(4)$	$2.421(4)$	1.112
27	$3s^2 3p^2 3d(^3P)^4P_{3/2}$	$0.72(27) + 0.49(38)$	$0.52(27) + 0.25(38)$	$1.811(4)$	$-7.991(3)$	1.513
28	$3s^2 3p^2 3d(^3P)^4P_{1/2}$	$-0.74(28) - 0.39(33)$	$0.55(28) + 0.15(33)$	$6.955(4)$	$0.000(0)$	2.188
29	$3s^2 3p^2 3d(^1D)^2G_{9/2}$	$0.87(29) + 0.47(20)$	$0.76(29) + 0.22(20)$	$1.298(4)$	$5.107(4)$	1.160
30	$3s^2 3p^2 3d(^1S)^2D_{3/2}$	$0.49(30) + 0.59(40)$	$0.23(30) + 0.33(40)$	$1.707(4)$	$1.130(4)$	0.989
31	$3s^2 3p^2 3d(^3P)^2D_{5/2}$	$0.68(31) - 0.44(35)$	$0.47(31) + 0.20(35)$	$1.069(4)$	$1.521(4)$	1.121
32	$3s 3p^4\ {}^2P_{1/2}$	$-0.59(32) - 0.44(22)$	$0.35(32) + 0.19(22)$	$4.212(3)$	$0.000(0)$	1.073
33	$3s^2 3p^2 3d(^1D)^2P_{1/2}$	$-0.77(33) - 0.38(39)$	$0.58(33) + 0.15(39)$	$-1.669(4)$	$0.000(0)$	0.925
34	$3s^2 3p^2 3d(^1D)^2D_{3/2}$	$0.75(34) + 0.38(9)$	$0.57(34) + 0.15(9)$	$1.355(4)$	$-9.406(3)$	0.978
35	$3s^2 3p^2 3d(^1D)^2D_{5/2}$	$-0.33(35) + 0.50(36)$	$0.11(35) + 0.24(36)$	$1.724(4)$	$-5.017(3)$	1.106
36	$3s^2 3p^2 3d(^1S)^2D_{5/2}$	$0.63(36) + 0.57(35)$	$0.40(36) + 0.32(35)$	$1.095(4)$	$3.925(4)$	1.192
37	$3s^2 3p^2 3d(^3P)^2F_{7/2}$	$0.78(37) - 0.54(26)$	$0.61(37) + 0.30(26)$	$1.632(4)$	$-4.412(3)$	1.131
38	$3s^2 3p^2 3d(^1D)^2P_{3/2}$	$0.65(38) + 0.48(12)$	$0.42(38) + 0.23(12)$	$9.234(3)$	$-8.137(3)$	1.225
39	$3s^2 3p^2 3d(^1D)^2S_{1/2}$	$0.70(39) + 0.38(13)$	$0.48(39) + 0.15(13)$	$9.066(4)$	$0.000(0)$	1.804
40	$3s^2 3p^2 3d(^3P)^2D_{3/2}$	$-0.71(40) + 0.35(30)$	$0.51(40) + 0.35(30)$	$1.016(4)$	$1.160(4)$	0.856
41	$3s^2 3p^2 3d(^3P)^2F_{5/2}$	$-0.44(41) + 0.60(31)$	$0.19(41) + 0.36(31)$	$1.102(4)$	$-2.070(4)$	1.102

range of 0.01–0.10 Å. The transition rates from VV and CV are generally in good agreement except for the transition $3s^2 3p^2 3d(^1D)^2D_{5/2}$–$3s^2 3p^3\ {}^2D_{3/2}$ with a transition rate of 3.0×10^9 s^{-1} which deviates from the VV and CV results by about two orders of magnitude.

To check the accuracy of the present data for the E1 transitions between the length and velocity forms of transition probabilities, $\log(A_l/A_v)$ as a function of the length form of transition probability A_l and as a function of line strength S_l were shown in Fig. 5a and b, respectively.

TABLE III

Spectral lines of Rb(XXIII), $a(b) = a \times 10^b$.

Upper level	Lower level	Wavelengths [Å]			Transition probabilities [s⁻¹]		
		Exp. [8]	CV	VV	Exp. [9]	CV	VV
$3s^23p^23d(^3P)^2F_{7/2}$	$3s^23p^3\,^2D_{5/2}$	103.556	103.459	103.021	2.1(11)	1.9(11)	2.0(11)
$3s^23p^23d(^1D)^2D_{5/2}$	$3s^23p^3\,^2D_{3/2}$	103.980	103.891	103.478	3.0(9)	1.0(11)	1.0(11)
$3s^23p^23d(^1D)^2D_{3/2}$	$3s^23p^3\,^2D_{3/2}$	104.469	104.376	103.919	1.3(11)	1.2(11)	1.3(11)
$3s^23p^23d(^3P)^4P_{3/2}$	$3s^23p^3\,^4S_{3/2}$	104.780	104.720	104.299	5.1(11)	1.5(11)	1.4(11)
$3s^23p^23d(^3P)^4P_{5/2}$	$3s^23p^3\,^4S_{3/2}$	106.357	106.298	105.851	1.5(11)	1.3(11)	1.5(11)
$3s^23p^23d(^1D)^2D_{5/2}$	$3s^23p^3\,^2D_{5/2}$	107.552	107.547	107.017	2.0(10)	6.6(10)	6.3(10)
$3s^23p^23d\,(^3P)^2D_{5/2}$	$3s^23p^3\,^2P_{3/2}$	109.510	109.423	108.916	1.8(11)	1.6(11)	1.7(11)
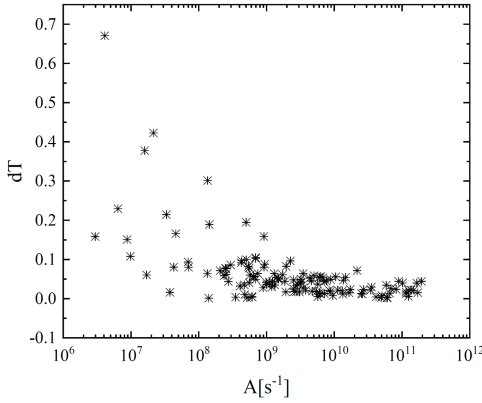
Fig. 6. A scatterplot of dT and A [s⁻¹] for all E1 transitions.
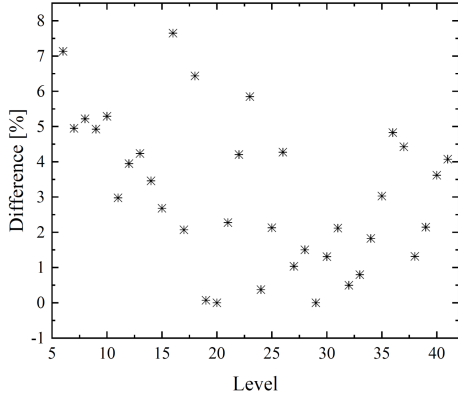
Fig. 7. A comparison of lifetime in length and velocity for Rb(XXIII).

The difference between A_l and A_v correlates with A-value much better than S-values, where the behavior of $\log(A_l/A_v)$ is regular with A-value (Fig. 5a), while the behavior with S-values is irregular (Fig. 5b).

Another check of the present data for the E1 transitions is the relative difference (dT) (d$T = \mathrm{abs}\,(A_l - A_v)/\max(A_l, A_v)$) between the transition rates in length and velocity gauges. A value close to d$T = 0$ for an allowed transition is a known accuracy indicator [20]. In many cases, the values are reasonably close to 0 (see Fig. 6).

TABLE IV

The uncertainty percentage for A of the E1 transition in Rb(XXIII).

Number of transitions	Uncertainty %	Uncertainty
6	4.55	AAA ($\leq 0.3\%$)
8	6.06	AA ($\leq 1\%$)
20	15.15	A+ ($\leq 2\%$)
17	12.88	A ($\leq 3\%$)
49	37.12	B+ ($\leq 7\%$)
17	12.88	B ($\leq 10\%$)
7	5.30	C+ ($\leq 18\%$)
4	3.03	C ($\leq 25\%$)
3	2.27	D+ ($\leq 40\%$)
1	0.76	D ($\leq 50\%$)

But in other cases, for example, the difference of the $3s^23p^23d(^3P)^4P_{3/2}$–$3s^23p^3\,^2P_{3/2}$ transition can be larger than 0.6. According to the uncertain estimation suggested by Kramida [21], the following averaged uncertainty for A values of E1 has been given in Table IV.

In particular, the presented calculations provide comprehensive new data for the E2, M1, and M2 transitions for Rb(XXIII), which no existent data for the public. This will help with the identification of spectral lines of Rb(XXIII). Owing to space limitations, full tables of the E1, E2, M1, and M2 transitions data will be provided by the authors on request.

The lifetime of the j level is represented as $\tau = 1/\left(\sum_j A_{ji}\right)$. Lifetime is a measurable datum, and it can be a good check on the accuracy of this calculation. The uncertainty of the lifetime value is calculated using $\frac{|\tau_l - \tau_v|}{\max(\tau_l, \tau_v)}$ and plotted in Fig. 7. The difference for all the excited levels considered here is up to ($\approx 3.13\%$). The present lifetime of the excited states from the CV $n = 7$ calculation, compared with the results from the $n = 7$ and $n = 6$ results $\frac{|\tau_{n=7} - \tau_6|}{\max(\tau_{n=7}, \tau_{n=6})}$ for the excited levels in Rb(XXIII), is presented in Fig. 8. The comparison shows good agreement between the two
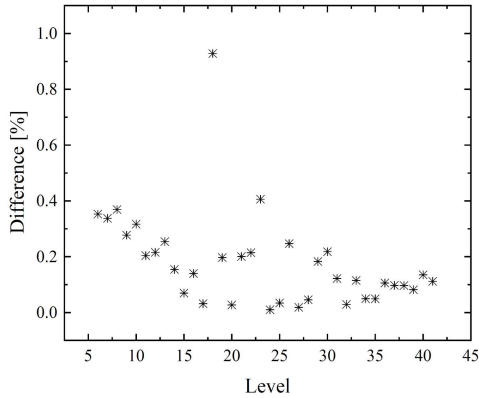
Fig. 8. A comparison of $\tau_{n=7}$ with $\tau_{n=6}$ for the excited levels in Rb(XXIII).

results, and the mean difference is within 0.30% except for the four excited levels, namely, $3s3p^4\ ^4P_{5/2}$ (0.35%), $3s3p^4\ ^4P_{3/2}$ (0.34%), $3s3p^4\ ^4P_{1/2}$ (0.37%), and $3s3p^4\ ^2D_{5/2}$ (0.32%).

4. Conclusion

Energy levels, oscillator strengths, and transition probabilities for E1, E2, M1, and M2 transitions are presented for the lowest 41 levels of Rb(XXIII) belonging to the $3s^23p^3$, $3s3p^4$, and $3s^23p^23d$ configurations. The valence–valence and core–valence correlation effects are accounted for systematically. The calculated energy levels and weighted oscillator strengths with the core–valence correlation effect show a good agreement with both theoretical and experimental data from the literature. The wavelengths are computed with almost spectroscopic accuracy, aiding line identification in spectra. Our results are useful for many applications such as astrophysics and atomic physics.

References

[1] S.A. Korotin, *Astron. Lett.* **46**, 541 (2020).

[2] M.P. Roriz, M. Lugaro, C.B. Pereira, N.A. Drake, S. Junqueira, C. Sneden, *Month. Notic. R. Astron. Soc.* **501**, 5834 (2021).

[3] C. Glaser, F. Karlewski, J. Kluge, J. Grimmel, M. Kaiser, A. Günther, H. Hattermann, M. Krutzik, J. Fortágh, *Phys. Rev. A* **102**, 012804 (2020).

[4] A. Zelenski, G. Atoian, D. Raparia, J. Ritter, D. Steski, *Rev. Sci. Instrum.* **87**, 02B705 (2016).

[5] J.E. Sansonetti, *J. Phys. Chem. Ref. Data* **35**, 301 (2006).

[6] A. Kramida, J.R. Fuhr, *Atomic Transition Probability Bibliographic Database*, National Institute of Standards and Technology, Gaithersburg (MD) 2020.

[7] J. Sugar, V. Kaufman, *J. Opt. Soc. Am. B* **1**, 218 (1984).

[8] J. Sugar, V. Kaufman, W.L. Rowan, *J. Opt. Soc. Am. B* **8**, 22 (1991).

[9] K.N. Huang, *At. Data Nucl. Data Tables* **30**, 313 (1984).

[10] E. Träbert, *Atoms* **2**, 15 (2014).

[11] P. Jönsson, G. Gaigalas, J. Bieroń, C. Froese Fischer, I.P. Grant, *Comput. Phys. Commun.* **184**, 2197 (2013).

[12] C. Froese Fischer, G. Gaigalas, P. Jönsson, J. Bieroń, *Comput. Phys. Commun.* **237**, 184 (2019).

[13] M.F. Gu, *Can. J. Phys.* **86**, 675 (2008).

[14] F. Hu, J.M. Yang, C.K. Wang, L.F. Jing, S.B. Chen, G. Jiang, H. Liu, L.H. Hao, *Phys. Rev. A* **84**, 042506 (2011).

[15] F. Hu, Y. Sun, M.F. Mei, C.C. Sang, *J. Appl. Spectrosc.* **85**, 749 (2018).

[16] I.P. Grant, *Relativistic Quantum Theory of Atoms and Molecules*, Springer, New York 2007.

[17] B.J. McKenzie, I.P. Grant, P.H. Norrington, *Comput. Phys. Commun.* **21**, 233 (1980).

[18] G. Gaigalas, C. Froese Fischer, P. Rynkun, P. Jönsson, *Atoms* **5**, 6 (2017).

[19] J. Gillaspy, *Trapping Highly Charged Ions: Fundamentals and Applications*, Nova Publ., Hauppauge (NY) 2001.

[20] J. Ekman, M. Godefroid, H. Hartman, *Atoms* **2**, 215 (2014).

[21] A. Kramida, *Astrophys. J. Suppl.* **212**, 11 (2014).